

Chapter 3

Phase-Shifting Interferometry and Combined Methods

3.1 Introduction

The chapter describes the hybrid phase-shifting full-field experimental CGS-photoelasticity method for in-plane tensorial stress determination and the experimental verification of the method. Section 3.2 presents the two experimental methods and how these are combined to determine the stress fields, detailing phase-shifting photoelasticity, the hybrid optical setup, and phase analysis methods. Section 3.3 describes the experimental verification of this method for stress determination in a compressed polycarbonate plate with a side V-notch and provides comparison with theoretical stress fields. This chapter is based on Kramer et al. (2009a), but provides more details of potential error sources and of the experimental analysis. Also, the comparison of experimental and theoretical stress fields has improved agreement upon further analysis after publication of the paper.

3.2 Phase-Shifting Interferometric Methods

3.2.1 Photoelasticity

Photoelasticity utilizes the stress-optic effect in certain materials that have a stress-induced birefringence proportional to the difference of the in-plane principal stresses: $n_1 - n_2 = c_o(\sigma_1 - \sigma_2)$, where c_o is the relative stress-optic coefficient. A detailed derivation of this equation may be found

in Appendix C. A photoelastic plate under stress acts as a linear retarder plate for polarized light with linear retardation δ with a fast axis at angle α relative to the x axis. The change in refractive index in the plane perpendicular to the optical axis is related to δ by the thickness of the plate h and the wavelength λ : $n_1 - n_2 = \delta\lambda/(2\pi h)$. Therefore, the governing equation, the Stress-Optic Law, may be written as the following (Kobayashi, 1993; Narasimhamurty, 1981):

$$\sigma_1 - \sigma_2 = \frac{\delta\lambda}{2\pi c_o h} = \frac{N\lambda}{c_o h}, \quad (3.1)$$

where $N = \delta/2\pi$ is the “fringe order”.

A circular polariscope used to view the photoelastic effect includes a polarizer with axis at angle ρ , a $\lambda/4$ plate with fast axis at angle ξ , the photoelastic material, another $\lambda/4$ plate with fast axis at angle ϕ , and a final polarizer with axis at angle β as shown in Figure 3.1.

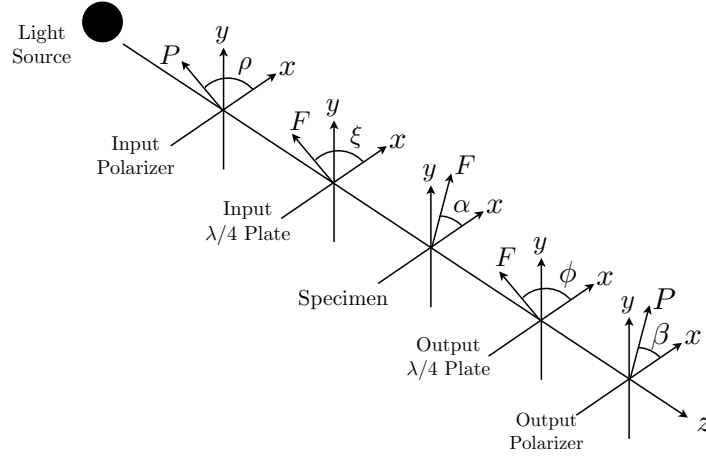


Figure 3.1: Schematic of circular polariscope with fast axes of optics labeled

The six-step method either has the input polarizer set to $\rho = \pi/2$ and the input $\lambda/4$ plate set to $\xi = 3\pi/4$ or has the input polarizer set to $\rho = 0$ and the input $\lambda/4$ plate set to $\xi = \pi/4$. The intensity for this general polariscope, calculated using Mueller Calculus as explained in Appendix C, is

$$I = I_o[1 + \cos(\delta) \sin(2(\beta - \phi)) - \sin(\delta) \sin(2(\alpha - \phi)) \cos(2(\beta - \phi))]. \quad (3.2)$$

Image	Intensity	ϕ	β
I_1	$I_o[1 + \cos(\delta)]$	$\pi/2$	$3\pi/4$
I_2	$I_o[1 - \cos(\delta)]$	$\pi/2$	$\pi/4$
I_3	$I_o[1 - \sin(\delta) \sin(2\alpha)]$	π	π
I_4	$I_o[1 + \sin(\delta) \cos(2\alpha)]$	$\pi/4$	$\pi/4$
I_5	$I_o[1 + \sin(\delta) \sin(2\alpha)]$	$\pi/2$	$\pi/2$
I_6	$I_o[1 - \sin(\delta) \cos(2\alpha)]$	$3\pi/4$	$3\pi/4$

Table 3.1: Photoelasticity phase shifting: Angles refer to fast axes of optics

With six combinations of the ϕ and β , the six-step method produces two images including only δ and four images including both δ and α , given in Table 3.1.

The isoclinic angle emerges from I_3 through I_6 in Equation (3.3) with wrapped phase range of $-\pi/4 \leq \alpha < \pi/4$:

$$\alpha = \frac{1}{2} \arctan \left(\frac{I_5 - I_3}{I_4 - I_6} \right) = \frac{1}{2} \arctan \left(\frac{\sin(2\alpha) \sin(\delta)}{\cos(2\alpha) \sin(\delta)} \right). \quad (3.3)$$

This wrapped α is only true for $\sin(\delta) \neq 0$; regions near $\sin(\delta) = 0$ will falsely appear to have α close to $\pm\pi/4$ since the argument to the $\arctan()$ in Equation (3.3) will grow very large as $\sin(\delta) \rightarrow 0$, as will be discussed in Section 3.3.1. By definition, the isoclinic angle may represent the angle between the reference axis and either σ_1 direction or σ_2 direction, a fact known as the isoclinic ambiguity (Siegmann et al., 2005). From the $\arctan()$ function in Equation (3.3), the wrapped isoclinic angle has $\pi/2$ discontinuities that are the boundaries between regions referring to σ_1 and σ_2 . Unwrapping the isoclinic angle by removing the $\pi/2$ discontinuities by adding $\pm\pi/2$ to appropriate regions produces a field that refers to only one of the principal stresses. These unwrapped isoclinic angles are allowed to contain π discontinuities since these are consistent with a reference to only one principal stress.

The isochromatic phase in Equation (3.4) uses all six images and the unwrapped isoclinic angle, producing a wrapped phase with range $-\pi \leq \delta < \pi$:

$$\delta = \arctan \left(\frac{(I_5 - I_3) \sin(2\alpha) + (I_4 - I_6) \cos(2\alpha)}{I_1 - I_2} \right). \quad (3.4)$$

If the wrapped isoclinic angle is used in Equation (3.4), then the resulting isochromatic phase may

be modulated (i.e., ambiguous), meaning some regions are related to $\sigma_1 - \sigma_2$ and other regions are related to $\sigma_2 - \sigma_1$, evident in the wrapped phase by poor fringe contrast and a sudden change in sign. This modulated/ambiguous isochromatic data is due to the isoclinic ambiguity such that α relative to σ_1 produces the $\sigma_1 - \sigma_2$ isochromatic regions and α relative to σ_2 produces the $\sigma_2 - \sigma_1$ isochromatic regions. The isochromatic phase may be demodulated by a load stepping method, which takes advantage of the change in δ at each point over three successive incremental loads (Ekman and Nurse, 1998; Ramesh and Tamrakar, 2000), by an automated digital technique that identifies and corrects the ambiguous zones before analysis (Ashokan and Ramesh, 2006), or by unwrapping the isoclinic angle (Siegmann et al., 2005). The load stepping method is not useful in an experiment that is sensitive to incremental loads as is the case with fracture, so it is not pursued for this proposed hybrid experimental method. The automated digital technique can be prone to error when poor quality data pixels are near the boundaries of the ambiguous zones, and this technique does not unwrap the isoclinic angle. Unwrapping the isoclinic angle can be complicated by the $\sin(\delta) \approx 0$ regions and by the allowance of π discontinuities such that careful choice in unwrapping algorithms is required, as will be discussed in Section 3.2.4.1.

For the combined CGS-photoelasticity method, a non-polarizing beamsplitter is positioned after the specimen to split the light for the two techniques, as further explained in Section 3.3. The incident face of the beamsplitter is aligned to be perpendicular to the light, resulting in a transmitted wavefront and a reflected wavefront that is perpendicular to the original propagation direction. The effect of a beamsplitter on polarized light can be modeled as a partial linear polarizer with transmission coefficients, T_x and T_y , and reflection coefficients, R_x and R_y , assuming the principal axes of the beamsplitter are aligned with the Cartesian axes; a similar model is used in a simultaneous capture phase-shifting photoelasticity technique developed by Patterson and Wang (1998). The transmitted beam is used for photoelasticity, and, thus, T_x and T_y affect the intensity of the modified

circular polariscope, calculated using Mueller calculus, as follows:

$$I = \frac{I_o}{2} [M_1 + M_2 \cos(\delta) - M_3 \sin(\delta) \sin(2\alpha) + M_4 \sin(\delta) \cos(2\alpha)] \quad (3.5a)$$

$$M_1 = (T_x + T_y) + (T_x - T_y) \cos(2\phi) \cos(2(\beta - \phi)) \quad (3.5b)$$

$$M_2 = 2\sqrt{T_x T_y} \sin(2(\beta - \phi)) \quad (3.5c)$$

$$M_3 = (T_x - T_y) + (T_x + T_y) \cos(2\phi) \cos(2(\beta - \phi)) \quad (3.5d)$$

$$M_4 = 2\sqrt{T_x T_y} \sin(2\phi) \cos(2(\beta - \phi)). \quad (3.5e)$$

With the prescribed angles for the output $\lambda/4$ plate and polarizer given in Table 3.1, the six-step phase-shifted images have intensities shown in Table 3.2.

Image	Intensity
I_1	$(I_o/2)[(T_x + T_y) + 2\sqrt{T_x T_y} \cos(\delta) - (T_x - T_y) \sin(\delta) \sin(2\alpha)]$
I_2	$(I_o/2)[(T_x + T_y) - 2\sqrt{T_x T_y} \cos(\delta) - (T_x - T_y) \sin(\delta) \sin(2\alpha)]$
I_3	$I_o T_x [1 - \sin(\delta) \sin(2\alpha)]$
I_4	$(I_o/2)[(T_x + T_y) + 2\sqrt{T_x T_y} \sin(\delta) \cos(2\alpha) - (T_x - T_y) \sin(\delta) \sin(2\alpha)]$
I_5	$I_o T_y [1 + \sin(\delta) \sin(2\alpha)]$
I_6	$(I_o/2)[(T_x + T_y) - 2\sqrt{T_x T_y} \sin(\delta) \cos(2\alpha) - (T_x - T_y) \sin(\delta) \sin(2\alpha)]$

Table 3.2: Photoelasticity phase-shifted images for a field transmitted through a beamsplitter placed inbetween the specimen and the output $\lambda/4$ plate

Considering images I_3 through I_6 to obtain α , the argument of the $\arctan()$ function from Equation (3.3) becomes

$$\left(\frac{I_5 - I_3}{I_4 - I_6} \right) = \left(\frac{-(T_x - T_y) + (T_x + T_y) \sin(\delta) \sin(2\alpha)}{2\sqrt{T_x T_y} \sin(\delta) \cos(2\alpha)} \right). \quad (3.6)$$

If $T_x = T_y$, then $(T_x + T_y) = 2\sqrt{T_x T_y}$, which implies the images from the modified circular polariscope in Table 3.2 give the same argument of the $\arctan()$ function as in Equation (3.3) for calculating the isoclinic angle. With the isoclinic angle and the six images, the argument of the $\arctan()$ function

in Equation (3.4) becomes

$$\begin{aligned} \left(\frac{(I_5 - I_3) \sin(2\alpha) + (I_4 - I_6) \cos(2\alpha)}{I_1 - I_2} \right) = & \left(\frac{[(T_x + T_y) \sin^2(2\alpha) + 2\sqrt{T_x T_y} \cos^2(2\alpha)] \sin(\delta)}{2\sqrt{T_x T_y} \cos(\delta)} \right) \\ & - \left(\frac{(T_x - T_y) \sin(2\alpha)}{2\sqrt{T_x T_y} \cos(\delta)} \right). \end{aligned} \quad (3.7)$$

Assuming $T_x = T_y$ and $(T_x + T_y) = 2\sqrt{T_x T_y}$, the calculation for the isochromatic phase simplifies to Equation (3.4). Perfectly aligned non-polarizing beamsplitters ideally have $T_x = T_y$, but usually have a tolerance on $(T_x - T_y)$, such that $(T_x + T_y) \approx 2\sqrt{T_x T_y}$. Manageable error may occur where $\sin(\delta)$ is close to zero in the isoclinic angle since the numerator in Equation (3.6) will be a discrete number larger than the small denominator, such that a false $\pi/2$ discontinuity may appear. These regions are considered carefully to eliminate these false discontinuities, as explained in Section 3.2.4.1. The potential for error in the isochromatic phase is smaller than in the isoclinic angle since the $(T_x - T_y)$ term in Equation (3.7) does not dominate the other term for the range of δ .

Another possible source of error is the rotational misalignment of the polarization optics in the rotation optical mounts. If (i) the first polarizer is correctly aligned with the specimen coordinate system, (ii) the misalignments of the first $\lambda/4$ plate, the second $\lambda/4$ plate, and the second polarizer are e_1 , e_2 , and e_3 in radians, respectively, and (iii) the beamsplitter is not in the polariscope, then the general intensity for the polariscope with $\rho = \pi/2$ and $\xi = 3\pi/4 + e_1$ (or $\rho = 0$ and $\xi = \pi/4 + e_1$) is

$$\begin{aligned} I = I_o & \left(1 + \sin(2e_1) \{ \sin(\delta) \sin[2(\beta - \phi) + 2(e_3 - e_2)] \sin(2\alpha - 2e_1) \right. \\ & + \cos(\delta) \sin[2(\beta - \phi) + 2(e_3 - e_2)] \cos[2(\beta - \phi) + 2(e_3 - e_2)] \sin(2\alpha - 2e_1) \\ & + \cos[2(\beta - \phi) + 2(e_3 - e_2)] \cos[2(\alpha - \phi) - 2e_2] \cos(2\alpha - 2e_1) \} \\ & + \cos(2e_1) \{ \cos(\delta) \sin[2(\beta - \phi) + 2(e_3 - e_2)] \\ & \left. - \sin(\delta) \cos[2(\beta - \phi) + 2(e_3 - e_2)] \sin[2(\alpha - \phi) - 2e_2] \} \right). \end{aligned} \quad (3.8)$$

With the prescribed angles for the output $\lambda/4$ plate and polarizer given in Table 3.1 and considering

images I_3 through I_6 to obtain α , the argument of the $\arctan()$ function from Equation (3.3) becomes

$$\left(\frac{I_5 - I_3}{I_4 - I_6}\right) = \left(\frac{\cos(2e_1) \sin(\delta) \sin(2\alpha - 2e_2) + \sin(2e_1) \sin(2\alpha - 2e_1) \cos(2\alpha - 2e_2)}{\cos(2e_1) \sin(\delta) \cos(2\alpha - 2e_2) - \sin(2e_1) \sin(2\alpha - 2e_1) \sin(2\alpha - 2e_2)}\right). \quad (3.9)$$

The argument to the wrapped α equation does not depend on e_3 , the error of the output polarizer, but only on the misalignment of the $\lambda/4$ plates. As will be demonstrated in the theoretical data in the example in Section 3.3.2.2, the isoclinic angle is more sensitive to e_1 than to e_2 in terms of development of false phase discontinuities near $\sin(\delta) = 0$, while error due to e_2 results in a shift in the values of α by e_2 . When $\sin(\delta) = 0$, Equation (3.9) should be indeterminate with $0/0$, leading to a value of zero for $\arctan[(I_5 - I_3)/(I_4 - I_6)]$ in MATLAB®, but if $e_1 \neq 0$, then Equation (3.9) is a small number divided by a different small number, leading to values close to $\pm\pi/2$ for $\arctan[(I_5 - I_3)/(I_4 - I_6)]$. When $\sin(\delta)$ is close to zero and $e_1 \neq 0$, then Equation (3.9) will likely be a small number divided by a different small number or $0/0$ depending on the values for α and e_2 , leading to a combination of false phase discontinuities and false zero-crossings in the wrapped α field, which require correction before unwrapping. Methods for this correction are described in Section 3.2.4.1. Without correction, the unwrapping algorithm will incorrectly determine α , which will be apparent in phase ambiguities in the wrapped δ data. Since the isoclinic angle is more sensitive to e_1 than e_2 , then e_2 is assumed to be zero and e_1 is a small number on the order of $\pm\pi/90$ radians.

With the correction methods for the wrapped isoclinic angle, the resulting isoclinic angle data appears to propagate only modest global error, as shown in the error analysis in Section 3.3.2, indicating that the correction methods are successful and that assuming $T_x \approx T_y$, $e_1 \approx \pm\pi/90$, and $e_2 \approx 0$ are reasonable assumptions.

3.2.2 Coherent Gradient Sensing

As described in Chapter 2, CGS in transmission applied to photoelastic materials is different from CGS applied to optically isotropic materials, leading to interference patterns related to two phases φ_{sum} and φ_{diff} , not just one phase. Controlling the input electric field polarization and adding

phase shifting allows determination of the desired phase φ_{sum} related to the spatial derivative of $\sigma_1 + \sigma_2$. Using the same polarization optics for both control of the polarization input for CGS and for the photoelasticity polariscope demonstrates how these two techniques may be combined to investigate the same field of view of the specimen. Additionally, the same input optics for both techniques simplifies the experimental setup. Therefore, using a polarizer and $\lambda/4$ plate prior to the specimen allows for the circularly polarized light necessary for photoelasticity and for determining φ_{sum} with only four phase-shifted CGS images per shearing direction.

Since the combined technique includes a non-polarizing beamsplitter after the specimen, then the reflectance coefficients, R_x and R_y , should be considered in the CGS analysis. The intensity of the image given in Equation (2.16a) is derived without consideration of R_x and R_y ; the intensity is the sum of the intensities from the E_1 field and from the E_2 field, and this sum advantageously cancels several terms present in the individual intensities. With R_x and R_y modulating the amplitudes of terms in these two orthogonal fields, many terms will not exactly cancel if $R_x \neq R_y$; but, the relative amplitudes of these uncanceled terms are small, on the order of $(R_x - R_y)$, compared to that of the terms given in Equation (2.16a). Assuming $R_x \approx R_y$ is reasonable since the global error is small, as is evident in Section 3.3.2.

Another possible source of error in the CGS data is the misalignment of the first two polarization optics. Since the photoelastic data is sensitive to the alignment of the first $\lambda/4$ plate, determining the sensitivity of the CGS data to this misalignment is important as well. A misalignment of e_1 radians for the first $\lambda/4$ plate leads to slightly elliptically polarized light as opposed to circularly polarized light. Depending on which pair of angles used for the circularly polarized light from the photoelasticity setup, whether $\rho = 0$ and $\xi = \pi/4 + e_1$ or $\rho = \pi/2$ and $\xi = 3\pi/4 + e_1$, the general equation for the CGS images in Equation (2.16) becomes the following, where A_o is the amplitude of the electric field after the first polarizer:

$$I^{image} = I_o + I_{1o} \cos[\varphi_{sum} + \varphi_{diff}] + I_{2o} \cos[\varphi_{sum} - \varphi_{diff}] \quad (3.10a)$$

$$I_o = 2(A_o^{\pm 1})^2 \quad (3.10b)$$

for $\rho = 0$ and $\xi = \frac{\pi}{4} + e_1$:

$$I_{1o} = I_o \left\{ \frac{1}{2} \cos^2(\alpha) [1 + \sin^2(2e_1)] + \frac{1}{2} \sin^2(\alpha) \cos^2(2e_2) \right. \\ \left. + \cos(\alpha) \sin(\alpha) \cos \left[\arctan \left[\frac{1 - \sin(2e_1)}{1 + \sin(2e_1)} \right] + \frac{\pi}{4} \right] \right\} \quad (3.10c)$$

$$I_{2o} = I_o \left\{ \frac{1}{2} \sin^2(\alpha) [1 + \sin^2(2e_1)] + \frac{1}{2} \cos^2(\alpha) \cos^2(2e_2) \right. \\ \left. - \cos(\alpha) \sin(\alpha) \cos \left[\arctan \left[\frac{1 - \sin(2e_1)}{1 + \sin(2e_1)} \right] + \frac{\pi}{4} \right] \right\}, \quad (3.10d)$$

and for $\rho = \frac{\pi}{2}$ and $\xi = \frac{3\pi}{4} + e_1$:

$$I_{1o} = I_o \left\{ \frac{1}{2} \cos^2(\alpha) \cos^2(2e_2) + \frac{1}{2} \sin^2(\alpha) [1 + \sin^2(2e_1)] \right. \\ \left. + \cos(\alpha) \sin(\alpha) \cos \left[\frac{3\pi}{4} - \arctan \left[\frac{1 + \sin(2e_1)}{1 - \sin(2e_1)} \right] \right] \right\} \quad (3.10e)$$

$$I_{2o} = I_o \left\{ \frac{1}{2} \sin^2(\alpha) \cos^2(2e_2) + \frac{1}{2} \cos^2(\alpha) [1 + \sin^2(2e_1)] \right. \\ \left. - \cos(\alpha) \sin(\alpha) \cos \left[\arctan \left[\frac{3\pi}{4} - \arctan \left[\frac{1 + \sin(2e_1)}{1 - \sin(2e_1)} \right] \right] \right] \right\}. \quad (3.10f)$$

When rewriting this as a single interference pattern using Equation (2.17), the equation is not as simple as that for the exactly circularly polarized electric field such that

$$I^{image} = I_o + I_c \cos[\varphi_{sum} + \varphi_c] \quad (3.11a)$$

$$I_c = \sqrt{I_{1o}^2 + I_{2o}^2 + 2I_{1o}I_{2o} \cos(2\varphi_{diff})} \neq \cos(\varphi_{diff}) \quad (3.11b)$$

$$\varphi_c = \arctan \left[\frac{(I_{1o} - I_{2o}) \sin(\varphi_{diff})}{(I_{1o} + I_{2o}) \cos(\varphi_{diff})} \right] \neq 0. \quad (3.11c)$$

The resulting wrapped phase from Equation (2.21) in this case is close to φ_{sum} since φ_c is small for small e_1 , but in fact, the wrapped phase is $\varphi_{sum} + \varphi_c$. Additionally, the wrapped phase may have some modulation by I_c where $I_c = 0$, since poor fringe contrast occurs where $\cos(\varphi_{diff}) \rightarrow 0$, which will be shown theoretically in the example below in Section 3.3.2.3. This e_1 error will mainly result in some unwrapping errors locally where $\cos(\varphi_{diff}) \rightarrow 0$ and will not greatly affect determining derivatives of $\sigma_1 + \sigma_2$ from the phase maps because for these applications $|\varphi_{sum}| \gg \varphi_c$. Despite this error source, the resulting phase maps will generally be a good representation of φ_{sum} for each

shearing direction, as shown in the example with small global error in Section 3.3.2.

3.2.3 Combined Experimental Setup

Experimentally, as shown in Figure 3.2, CGS and photoelasticity can be employed simultaneously by sending a plane wave of coherent monochromatic light through the input polarizer, the input $\lambda/4$ plate, and the specimen, after which the light is split by a non-polarizing beamsplitter into two identical wavefronts sent along two separate sets of analyzing optics, one for CGS and the other for photoelasticity. Identical imaging optics and CCD cameras are used to capture the same field of view of the specimen for each technique. Another option for combining these techniques is to replace the non-polarizing beamsplitter with a translating mirror at 45° to the incoming deformed light after the specimen; to perform photoelasticity, the translating mirror is out of the beam path to allow all of the light to pass through the remaining photoelasticity optics, and to perform CGS, the translating mirror is moved into the beam path to turn the light to pass through the CGS optics. The translating mirror option removes the errors associated with the non-polarizing beamsplitter.

The light is collimated using a spatial filter, consisting of a microscope objective and a pinhole, and a collimating lens placed at one focal length of the collimating lens from the pinhole. The polarizers and $\lambda/4$ plates are mounted in rotation stages with 1° markings, though the user must align the fast axis fiducial marking on the optic casing with the rotation mount markings by hand. Rotational alignment is achieved by first setting the first polarizer as the standard, and methods for extinguishing the light detected on a CCD are used to set the alignment of the other polarization optics. To obtain each of the six photoelasticity images, the output $\lambda/4$ plate and polarizer must be adjusted manually. In order to induce the $\pi/2$ phase shift for the CGS data, the first Ronchi grating is translated a distance of $p/4$ by 1D piezoelectric positioners, one for each shearing direction. To obtain the two shearing directions for the same load of the specimen, one set of phase-shifted images for one shearing direction is taken, and then the Ronchi gratings are rotated by $\pi/2$ and the imaging optics and filter plane are adjusted to capture the phase-shifted images for the other shearing direction. In the current configuration, the images for both shearing directions and photoelasticity cannot

be obtained simultaneously, though this may be achieved with other optical solutions described in Chapter 5.

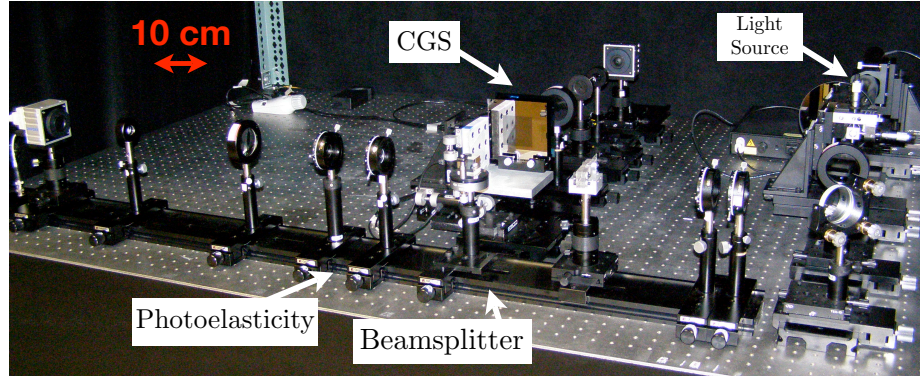
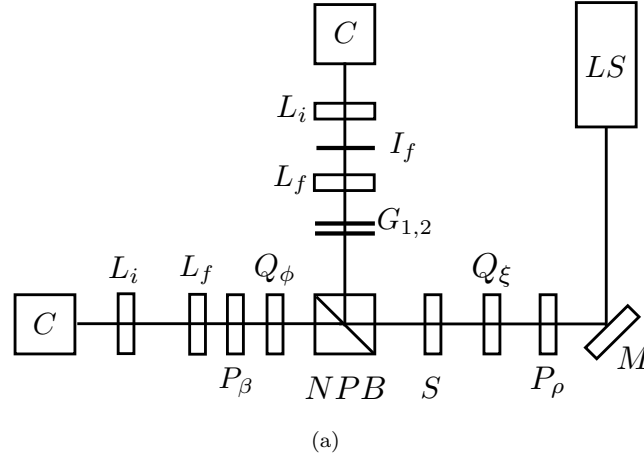


Figure 3.2: Combined CGS-photoelasticity experimental setup: (a) Schematic of the experimental setup: LS =light source with collimation optics; M =mirror; P =polarizer; $Q=\lambda/4$ plate; S =specimen; NPB =non-polarizing beamsplitter; $G_{1,2}$ =gratings 1&2; L_f =filtering lens; I_f =filtering iris diaphragm; L_i =imaging lens; and C =camera; and (b) image of experimental setup from side view of photoelasticity optics

3.2.4 Full-Field Phase Unwrapping and Integration

The data analysis is performed using an analysis program written using MATLAB[®]. The 2D phase unwrapping method for both photoelastic and CGS data is the PCG algorithm described in Chapter 2. Phase unwrapping of the experimental isoclinic angle requires special care where, prior to unwrapping by the PCG algorithm, the wrapped data is corrected for errors that are due to the

non-polarizing beamsplitter and to alignment of the polarization optics as explained in Section 3.2.1. The PCG algorithm may also be applied to numerically integrate the spatial derivatives of $\sigma_1 + \sigma_2$.

3.2.4.1 Phase Unwrapping for the Isoclinic Angle

In the wrapped isoclinic data from Equation (3.3), regions where $\sin(\delta) = 0$ are undefined. These regions may be identified using the isochromatic data. Near $\sin(\delta) = 0$, both the numerator and denominator of the isoclinic $\arctan()$ formula in Equation (3.3) are close to zero, but with slightly different small numbers from the nonzero tolerance on $(T_x - T_y)$ and misalignment of the polarization optics. These regions ultimately may appear as false $\pi/2$ discontinuity regions in the wrapped isoclinic angle. Additionally, regions where the numerator and the denominator of the $\arctan()$ formula are zero, MATLAB® will return a value of zero for the $\arctan()$, but these points may also require correcting since the isoclinic angle is not necessarily zero at those locations.

With a user-defined threshold value, denoted *thresh*, then the data in zones where $-\text{thresh} < \sin(\delta) < \text{thresh}$ are identified as likely locations where the data needs correction. The δ used here is the ambiguous wrapped isochromatic phase, described in Section 3.2.1, because this comes from using wrapped α in the formula for wrapped δ in Equation (3.4). The ambiguous wrapped isochromatic phase is a key tool to correcting the wrapped isoclinic angle because the ambiguous wrapped δ should ideally have (i) good phase discontinuities of height 2π that require unwrapping, (ii) continuous phase, or (iii) boundaries of the ambiguous data having opposite sign across the boundaries (where the boundaries of $\sigma_1 - \sigma_2$ and $\sigma_2 - \sigma_1$ regions meet). Phase discontinuities of height 2π and zero-crossings in the wrapped δ correspond to where $\sin(\delta) \approx 0$, so these are precisely where the isoclinic angle data has possible problems. The ambiguity boundaries in the wrapped δ should coincide with the $\pi/2$ phase discontinuities in the wrapped α , which are true wrapped phase discontinuities that must be preserved.

The following are some basic guidelines to correcting the isoclinic angle, but the user must apply judgment, informed by the expected form of the wrapped α and δ , in cases where no single guideline may be applied:

- If the $\pi/2$ phase discontinuity in the wrapped α coincides with an ambiguity boundary in the wrapped δ , then this discontinuity should be preserved and left alone.
- If both the wrapped α and wrapped δ are continuous, and if the wrapped delta is not near where $\sin(\delta) \rightarrow 0$, then this data should be left alone.
- If phase discontinuities from both wrapped α and wrapped δ coincide, then the phase discontinuity in α should be interpolated across.
- If a true $\pi/2$ phase discontinuity in the wrapped α *intersects* the location of a wrapped δ discontinuity, great care must be taken when interpolating across the false α discontinuity while preserving the true α discontinuity.
- If a $\sin(\delta) \rightarrow 0$ region coincides with a zero-crossing in the wrapped α , then this zero-crossing is likely near where wrapped α is actually close to $\pm\pi/4$. These types of zero-crossings are often where both $\sin(\delta)$ and $\cos(2\alpha)$ are close to zero, leading to a $0/0$ as the argument of the α $\arctan()$ formula. The user can insert a phase discontinuity in this region. Another indication for this case is that the ambiguous wrapped δ does not have a phase discontinuity, but a change of direction about $\pm\pi$; this change of direction should be a phase discontinuity that connects to another phase discontinuity in the wrapped δ field.
- Phase discontinuities in α need to either connect or end on a boundary; they should not end in the middle of the field.

Once false phase discontinuities are identified, then these are removed from the wrapped field and replaced with data from 2D linear interpolation across those zones. Then the modified wrapped isoclinic data is unwrapped using the PCG algorithm.

This unwrapped isoclinic angle is used in Equation (3.4) for the unambiguous wrapped isochromatic phase. The wrapped δ calculated from the unwrapped α should not contain phase ambiguities and should only contain continuous phase or phase discontinuities of height 2π ; if this is not the case, then the wrapped isoclinic angle was not properly modified and requires correction.

Since the sign of the numerator and of the denominator of the $\arctan()$ function in Equation (3.4) are known separately, then the full four quadrants of $\arctan()$ phase space may be used, resulting in an isochromatic wrapped phase with range $-\pi \leq \delta < \pi$. Having 2π phase discontinuities instead of π discontinuities reduces the density of discontinuities in the entire field, reducing the computational effort to unwrap the field. For both the isoclinic angle and the CGS phases, unwanted phase information modulates the numerator and denominator, which implies the sign of the numerator and denominator of the $\arctan()$ function are not known independently. Thus the $\arctan()$ formula produces a phase with a range from $-\pi/2$ to $\pi/2$, giving wrapped phase ranges of $-\pi/4 \leq \alpha < \pi/4$ and $-\pi/2 \leq \varphi_{sum} < \pi/2$.

3.2.4.2 Preconditioned Conjugate Gradient Method for Integration

Letting $s = (\sigma_1 + \sigma_2)$, the solutions to the phase unwrapping for the horizontal and vertical shearing directions result in $\partial s / \partial x$ and $\partial s / \partial y$, which must be integrated to obtain s . This integration problem is a discrete Poisson equation of the form:

$$\begin{aligned}
 (s_{i+1,j} - 2s_{i,j} + s_{i-1,j}) + (s_{i,j+1} - 2s_{i,j} + s_{i,j-1}) \\
 = \left[\left(\frac{\partial s}{\partial x} \right)_{i,j} - \left(\frac{\partial s}{\partial x} \right)_{i-1,j} \right] \Delta x \\
 + \left[\left(\frac{\partial s}{\partial y} \right)_{i,j} - \left(\frac{\partial s}{\partial y} \right)_{i,j-1} \right] \Delta y, \quad (3.12)
 \end{aligned}$$

where Δx and Δy are the specimen distance per pixel. Assuming Neumann boundary conditions, Equation (3.12) may be solved by the same PCG algorithm used for the phase unwrapping with a weight function, \mathbf{W} , that is the product of the quality weight functions from the unwrapping in the horizontal and vertical directions.